ORIGINAL ARTICLES

# COMPARISON OF OPTICAL-SPECTRAL CHARACTERISTICS OF GLIOBLASTOMA AT INTRAOPERATIVE DIAGNOSIS AND *EX VIVO* OPTICAL BIOPSY

**Romanishkin I.D.[1], Savelieva T.A.[1,2], Ospanov A.[2], Kalyagina N.A.[1,2], Krivetskaya A.A.[1,2], Udeneev A.M.[2], Linkov K.G.[1], Shugay S.V.[3], Pavlova G.V.[3,4], Pronin I.N.[3], Loschenov V.B.[1,2]**
[1]Prokhorov General Physics Institute of Russian Academy of Sciences, Moscow, Russia
[2]National Research Nuclear University MEPhI, Moscow, Russia
[3]N.N. Burdenko National Medical Research Center of Neurosurgery, Moscow, Russia
[4]Institute of Higher Nervous Activity and Neurophysiology of the Russian Academy of Sciences, Moscow, Russia

## Abstract

The difficulty of intraoperative delineation of glial tumors is due to the peculiarities of their growth along vessels and nerve fibers with infiltration of healthy white matter. Insufficiently complete removal of tumor tissues leads to recurrences, and excessive removal is fraught with neurological complications. Optical spectroscopy methods are characterized by high speed, accuracy and non-invasiveness, which determines the prospects of their use for intraoperative demarcation of the boundaries of such tumors. Fluorescence and diffuse reflectance spectroscopy have found wide application in intraoperative neuronavigation, mainly for detecting the edges of diffuse gliomas. At the same time, in recent years the direction of *ex vivo* spectral analysis of tumor samples using a combination of various optical spectroscopy methods, including both elastic and inelastic scattering spectroscopy, has been actively developed. Obviously, the ability to obtain spectra intraoperatively and on fresh specimens is different. The present article compares the results of the analysis of optical-spectral characteristics of intracranial tumors at intraoperative diagnosis and *ex vivo* analysis and proposes a mathematical model for interpretation of the observed dependencies.

**Keywords**: glial tumors, optical spectroscopy, scattering, mathematical modeling, Monte Carlo simulation.

**Contacts**: Romanishkin I.D., e-mail: igor.romanishkin@nsc.gpi.ru.

**For citations**: Romanishkin I.D., Savelieva T.A., Ospanov A., Kalyagina N.A., Krivetskaya A.A., Udeneev A.M., Linkov K.G., Shugay S.V., Pavlova G.V., Pronin I.N., Loschenov V.B. Comparison of optical-spectral characteristics of glioblastoma at intraoperative diagnosis and *ex vivo* optical biopsy, *Biomedical Photonics*, 2024, vol. 13, no. 4, pp. 4–12. doi: 10.24931/2413–9432–2024–13–4–4–12

# СРАВНЕНИЕ ОПТИКО-СПЕКТРАЛЬНЫХ ХАРАКТЕРИСТИК ГЛИОБЛАСТОМЫ ПРИ ИНТРАОПЕРАЦИОННОЙ ДИАГНОСТИКЕ И ОПТИЧЕСКОЙ БИОПСИИ *EX VIVO*

**И.Д. Романишкин[1], Т.А. Савельева[1,2], А. Оспанов[2], Н.А. Калягина[1,2], А.А. Кривецкая[1,2], А.М. Уденеев[2], К.Г. Линьков[1], С.А. Горяйнов[3], С.В. Шугай[3], Г.В. Павлова[3,4], И.Н. Пронин[3], В.Б. Лощенов[1,2]**
[1]Институт общей физики им. А.М. Прохорова Российской академии наук, Москва, Россия
[2]Национальный исследовательский ядерный университет «МИФИ», Москва, Россия
[3]Национальный медицинский исследовательский центр нейрохирургии имени академика Н. Н. Бурденко, Москва, Россия
[4]Институт высшей нервной деятельности и нейрофизиологии Российской академии наук, Москва, Россия

## Резюме

Сложность интраоперационного определения границ глиальных опухолей обусловлена особенностями их роста вдоль сосудов и нервных волокон с инфильтрацией здорового белого вещества. При этом недостаточно полное удаление опухолевых тканей приво-

дит к рецидивам, а избыточное удаление чревато неврологическими осложнениями. Методы оптической спектроскопии характеризуются высокой скоростью, точностью и неинвазивностью, что обуславливает перспективность их использования для интраоперационной демаркации границ таких опухолей. Спектроскопия флуоресценции и диффузного отражения нашли широкое применение в интраоперационной нейронавигации, главным образом, для обнаружения краев диффузных глиом. При этом в последние годы активно развивается направление *ex vivo* спектрального анализа образцов опухолей с помощью сочетания различных методов оптической спектроскопии, включающих спектроскопию как упругого, так и неупругого рассеяния. Очевидно, возможности регистрации спектров при интраоперационной работе и на свежих образцах отличаются. В настоящей статье проведено сравнение результатов анализа оптико-спектральных характеристик внутричерепных опухолей при интраоперационной диагностике и анализе *ex vivo*, а также предложена математическая модель для интерпретации наблюдаемых зависимостей.

**Ключевые слова**: глиальные опухоли, оптическая спектроскопия, рассеяние, математическое моделирование, Монте-Карло моделирование.

**Контакты**: Романишкин И.Д. e-mail: igor.romanishkin@nsc.gpi.ru.

**Для цитирования**: Романишкин И.Д., Савельева Т.А., Оспанов А., Калягина Н.А., Кривецкая А.А., Уденеев А.М., Линьков К.Г., Горяйнов С.А., Шугай С.В., Павлова Г.В., Пронин И.Н., Лощенов В.Б. Сравнение оптико-спектральных характеристик глиобластомы при интраоперационной диагностике и оптической биопсии *ex vivo* // Biomedical Photonics. – 2024. – Т. 13, № 4. – С. 4-12. doi: 10.24931/2413–9432–2024–13–4–4–12

## Introduction

Currently, the primary line of therapy for highly malignant brain tumors is surgical resection, but *in vivo* tumor delineation remains a major challenge. Recent technological advances in neurophotonic developments such as Raman spectroscopy, thermal imaging, optical coherence tomography, and fluorescence spectroscopy have enabled the development of techniques for minimally invasive neurosurgery [1]. Despite advances in optical techniques, biopsy analysis remains the standard diagnostic tool for tumor delineation.

Further development of intraoperative analysis techniques with visual inspection would provide neurosurgeons with real-time information, shorten surgical procedure time, and enable more accurate resection by detecting residual or hidden tumor foci. Visual inspection tools can view and analyze the location, size, shape, type, and extent of tumors [1–6].

Among the promising new optical techniques for cancer diagnosis with the possibility of intraoperative tissue assessment is Diffuse Reflectance Spectroscopy (DRS). DRS is a non-invasive or minimally invasive technique that typically uses separate optical fibers – to deliver broadband light to the tissue and to register diffusely reflected light with a spectrometer. Diffuse reflectance signal formation is possible because biological tissues are characterized by their ability to scatter light multiple times, resulting in light scattering from the source in all directions, with a portion of the scattered light returning back. DRS can provide such clinical information as total hemoglobin content, tissue oxygen saturation, tissue lipid and water content, and tissue scattering properties. The method has already been used, for example, in studies to classify tumor tissue in upper gastrointestinal cancers [7], to distinguish tumor tissue from fibrosis in patients with rectal cancer as a guide to surgery [8], and to record optical mammograms and quantify absorption and scattering properties, from which hemoglobin concentration and oxygen saturation of healthy and pathological breast tissue were obtained and analyzed [9]. Studies have shown that DRS can aid in intraoperative decision-making during cancer surgery, including selecting the best resection plane and area, and distinguishing fibrotic or healthy tissue from tumor tissue.

In neurosurgery, the DRS method has been used to assess blood fractions and oxygen saturation changes by spectroscopic signal and hemoglobin absorption spectrum [10], to distinguish between glial tumors and normal brain *ex vivo* by assessing DRS signal [11], and to detect cancer *in vivo* without labels and in real time during brain surgery [12].

However, the accuracy of tissue classification is still insufficient and the DRS method requires further development. In this paper, we interpret a number of our findings on the diffuse light reflection spectra of intracranial tumor tissues and compare the data obtained *in vivo* during neurosurgical surgery for tumor removal, and *ex vivo* during biobanking. The results of the comparison allows avoiding methodological errors when translating such technologies. The mathematical model of elastic multiple scattering of light by the studied tissues proposed in the article allows to take into account not only karyomorphometric data, obvious in classical histological analysis with hematoxylin-eosin staining, but also demonstrates the necessity to take into account the contribution of larger structures, such as myelin sheaths of nerves, as well as, on the contrary, smaller ones, such as subcellular structures, e.g. mitochondria.

## Materials and methods

### *Method and device for simultaneous registration of diffuse reflectance and fluorescence spectra in vivo*

Diffuse reflectance spectra of tumor tissues are the object of the present study. The fluorescence of 5-aminolevulinic acid (5-ALA) induced protoporphyrin IX (PpIX) was used as a marker of tumor changes in

the area of interest. In the process of post-processing of spectral data obtained in the clinic, we analyzed the co-distribution of PpIX and markers of structural changes determined by the diffuse reflectance spectrum.

For simultaneous registration of diffuse reflectance and fluorescence spectra, the device described in [13] was used. The emission from a broadband source (halogen lamp) was filtered through a 500–600 nm bandpass filter. A laser source with a wavelength of 632.8 nm (He-Ne laser) was used to excite the fluorescence. Diffuse reflectance and fluorescence spectra were recorded simultaneously in 500–640 and 640–850 nm spectral ranges, respectively. Measurements were performed using a fiber-optic probe, the illumination and the receiving fibers were collected in a special bundle and placed on one side of the object, which determined the specifics of signal registration in the diffuse reflectance geometry (Fig. 1). Several hours before the operation, a solution of 5-ALA hydrochloride was injected into the patient's body. The combined spectra of normal tissue (usually the cerebral cortex at a distance from the tumor projection) and pathologically altered tissue above the tumor, in the tumor, and in the tumor bed (to control the quality of the resection) were measured sequentially during the tumor resection surgery. This paper presents a retrospective analysis of *in vivo* data obtained at the Burdenko Neurosurgery Center. Diffuse reflectance spectra recorded during the removal of glioblastomas (in 38 patients, 163 samples in total) and anaplastic astrocytomas (in 6 patients, 35 samples in total) were considered. Glioblastoma samples were distributed as follows: 14 samples with normally appearing white matter (NAWM), 18 samples from the perifocal area of tumor, 86 samples from tumor center, 18 samples with necrotic tissues. Anaplastic astrocytoma samples included 21 samples from tumor center, 11 – from perifocal area, 3 NAWM, and no necrosis.

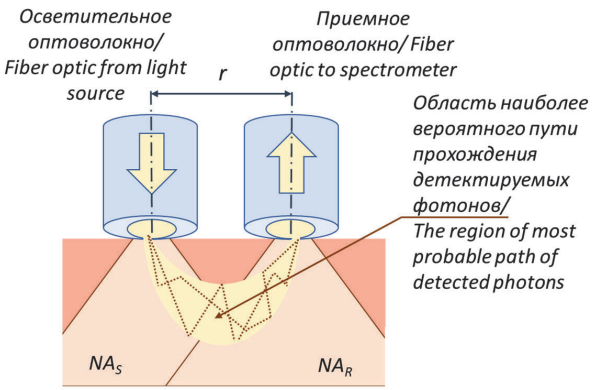


**Рис. 1.** Схема регистрации сигнала диффузного отражения: r – расстояние от центра осветительного волокна до центра приемного волокна, $NA_s$ – числовая апертура осветительного волокна, $NA_R$ – числовая апертура приемного волокна.
**Fig. 1.** Scheme of registration of diffuse reflection signal: r – distance from the center of the illumination fiber to the center of the receiving fiber, $NA_s$ – numerical aperture of the illumination fiber, $NA_R$ – numerical aperture of the receiving fiber.

***Method and device for simultaneous recording of diffuse reflectance and Raman spectra ex vivo***

Studies of the combined method of *ex vivo* optical biopsy of tumor samples were conducted in the laboratory of neurosurgical anatomy and preservation of biological materials at the Burdenko Neurosurgery Research Center on tumor tissue samples extracted during neurosurgical operations, immediately after removal. Samples from patients diagnosed with glioblastoma (n=60) were studied. From each patient 1–4 biopsy specimens were taken with subsequent verification by pathomorphologic examination (84 specimens in total).

For all samples, Raman spectra were measured with StellarNet Raman-HR-TEC-785 spectrometer under 785 nm excitation, fluorescence was measured at 405 nm and 632.8 nm, and diffuse reflectance was measured in 500–600 nm spectral range using Biospec LESA-01-BIOSPEC spectrometer. In this paper, we use only diffuse reflectance spectroscopy data in white light (to calculate hemoglobin concentration) and at 632.8 nm, just as we did in *in vivo* measurements performed in the operating room. The results of our previous studies of this method [14–16] showed a significant contribution of these spectroscopic features to the principal components.

***Algorithm for processing diffuse reflectance spectra***

Raman, fluorescence, and diffuse reflectance spectra were subjected both to preprocessing in order to increase decoding properties and to various variants of decomposition in order to highlight characteristic features peculiar to the tissues under study.

From the fluorescence spectrum of PpIX, we calculated the values of the 632.8 nm integral backscatter laser intensity (area under the spectrum curve in the range of 625–640 nm) and the value of the PpIX fluorescence index (ratio of the area under the spectrum curve in the range of 690–730 nm to the value of the 632.8 nm integral laser intensity). In this work, we consider only the first of these parameters.

The spectrum of diffusely reflected by the tissue broadband light was used to calculate the hemoglobin concentration [17] in the sample and the light scattering coefficient [18].

***Model of light interaction with structural elements of tumor tissues***

To determine the influence of the measurement geometry and biological processes occurring in the tumor on the recorded signals, a mathematical model of the studied biological tissue in different states was developed. It considered both the variation of individual tissue components using Mie theory and their concentration and composition of the medium, for which the Monte Carlo simulation method was chosen, which has a higher accuracy in the tissue regions proximal

to the illuminator and receiver than the diffusion approximation of the radiative transfer theory [19].

Cells, organelles, elements of intercellular matrix, nerve endings can be approximated by spheres and cylinders with refractive indices corresponding to the content of proteins and fats in them, and immersed in a medium whose refractive index is determined by all the molecules contained in it that are not accounted for as independent scatterers. The scattering cross section of unpolarized light by a spherical particle was determined according to [20]. The infinite cylinder solution, also proposed by Bohren and Huffman, was used to model the scattering of an electromagnetic wave on myelinated nerve fibers. Two variants of wave incidence with respect to the plane in which the cylinder lies: parallel and perpendicular to the plane of incidence, were considered and averaged.

***Numerical modeling of radiation propagation in scattering and absorbing media***

The Monte Carlo method is widely used for numerical solution of the radiative transfer theory (RTT) equation, which is based on modeling of photon transport in a scattering medium. The initial conditions are set and each act of photon scattering on the inhomogeneities of the medium is traced up to its absorption or exit from the sample. Free path length and rotation angle are random variables with theory-based distribution. The scattering and absorption probabilities are determined by the $\mu_s'$ and $\mu_a$ coefficients. The main disadvantage of the Monte Carlo method is the substantial expenditure of computational resources, which renders it impractical for addressing the inverse problem in real time. However, it is possible to develop algorithms for data interpretation based on Monte Carlo simulation, as was done in [21] to describe the dependence of the diffuse reflection coefficient on the absorption and scattering coefficients for a semi-infinite medium.

In the present work, a Monte Carlo packet method has been implemented in the Visual Studio development environment using C# language tools. It is based on the assumption that a set of photons begins to co-propagate in the medium, but gradually the population of the packet runs out due to absorption, and the remaining part of the packet is scattered until the population of the packet becomes too small. This technique allows us to increase the dynamic range of the calculated distribution at unchanged costs of machine time in case of the absorbing medium. For registration of radiation the possibility of receiving radiation with a given aperture on a given area at a given distance from the source in the XY plane is realized.

***Determination of input parameters of mathematical modeling***

The main characteristic of glial tumors is their growth along myelinated nerve fibers and blood vessels without forming a capsule, which leads to their infiltration into the normal white matter of the brain [22]. At the organ-tissue level, glial tumors consist of central and perifocal zones [23] and lead to displacement, deviation, and destruction of nerve tracts during their development [24]. The central zone of glioblastoma multiforme (the most malignant form of glial tumors) is characterized by the development of necrosis in the tumor nucleus with concomitant destructive changes of myelinated nerve fibers [25, 26].

At the tissue level, the number and shape of cell membranes should also be taken into account. It is well known that about 50% of the white matter consists of myelin sheaths of nerve tracts, which are multilayered membranes consisting of a lipid bilayer (70-85% of dry matter) with protein inclusions (15–30%) [27, 28], which causes its high refractive index. How developed the surface of the astrocyte membranes is also important, as this factor is altered by cell compaction in the tumor and affects scattering.

In [29], diffusion tensor MRI was used to show that fluctuations in the fractional anisotropy index correlate with the integrity of nerve tracts formed by myelinated fibers, as well as with the state of the cells. Thus, the significant decrease of the fractional anisotropy index in the center of glioblastoma is due to a high degree of nerve fiber disintegration and necrotic changes, while its more moderate deviations are observed in the perifocal zone, where nerve tracts are still structured and intact glia

**Таблица 1**
**Результаты исследования показателя фракционной анизотропии для глиальных опухолей различной степени озлокачествления**

**Table 1**
**Results of the fractional anisotropy index study for glial tumors with different degrees of malignancy**

| Центр опухоли Tumor center | Граница Edge | Нормальное белое вещество Normal white matter | Источник Reference |
|---|---|---|---|
| **Глиобластома (IV стадия) Glioblastoma (Grade IV)** | | | |
| | 0.257 | 0.467 | [30] |
| 0.13 | 0.16 | 0.47 | [26] |
| 0.13 | 0.2085 | 0.4685 | среднее average |
| **Анапластическая астроцитома (III стадия) Anaplastic astrocytoma (Grade III)** | | | |
| 0.165 | 0.168 | 0.391 | [31] |
| | 0.223 | 0.467 | [30] |
| 0.165 | 0.1955 | 0.429 | среднее average |
| **Диффузная астроцитома (II стадия) Diffuse astrocytoma (Grade II)** | | | |
| 0.144 | 0.259 | 0.391 | [32] |

cells are observed. The numerical values of this coefficient, averaged from data from the literature, are shown in Table 1.

For modeling purposes, to unify data from different sources, the fractional anisotropy index values obtained in each study were normalized for the tumor center and margin to the values from normal white matter. After that, the average values were calculated, which were reduced to the absolute value of the fractional anisotropy index by multiplication by its average value for normal white matter for all studies.

As can be seen in Table 2, at the cellular level, glioblastoma multiforme (Grade IV) exhibits such features as dense cellularity, atypical development of nuclei, increase in their size, and pleomorphism (diversity of shapes) [36]. Anaplastic astrocytoma is characterized by increased cell density, anaplasia, and mitosis, but to a lesser extent than glioblastoma. Benign tumors show a moderate increase in cell density and nuclei size without cellular atypia or mitotic activity [38, 39]. At the subcellular level, the most critical changes occur in the content and structure of mitochondria. In normal tissue, mitochondria make up about 7–8% of the cell volume [40, 41]. In liver tissue, mitochondria have been shown to have a significant effect on light scattering by the cell [42, 43]. Also, by analyzing liver slices using phase-contrast microscopy, Schmitt and Kumar showed a significant contribution of organelles to light scattering by cells [44].

## Results and discussion

### *Comparison of in vivo and ex vivo data*

The results of our previous work have shown that in the combined spectral analysis of glial tumor tissues, one of the most prominent features in classification is the intensity of diffuse light scattering [13, 16]. Results confirming this observation were obtained in [12].

Our *in vivo* and *ex vivo* studies included different kinds of pathomorphological data, which determined the samples as coming from normal white matter, perifocal tumor area, or actively growing part of tumor, and the percentages of tumor and necrotic tissue in the sample (Fig. 2). In our *ex vivo* biobanking studies of optic-spectral characteristics, the samples were represented as having a certain percentage of tumor/connective/fibrotic/necrotic tissue. However, when we subdivide this sample into quartiles by tumor tissue content (with the exclusion of necrotic areas), we see a similar pattern of correlation between the degree of malignancy in the measured area and the scatter score. The lowest light-scattering values correspond either to the perifocal zone (in *in vivo* measurements) or to a tumor content of 25 to 50% in the sample (in *ex vivo* measurements), which are reasonable to compare with each other. Some differences in the distribution of light scattering in different types of glioblastoma tissues are also observed. For example, in *in vivo* measurements, we could afford to record spectral dependencies from normal white matter far away from the tumor, as this did not require its removal.

The healthy areas of white matter obtained in the biobanking process, were the areas adjacent to the tumor showing morphological signs of normality. However, according to the light-scattering ratio for *ex vivo* measurements, we can assume that these samples were still subject to some changes. Our mathematical model of the relevant structural changes occurring in neural tissues during tumor development is presented in the following section.

**Таблица 2**
Данные кариоморфометрии для глиальных опухолей различной степени озлокачествления
**Table 2**
Karyomorphometry data for glial tumors of different degrees of malignancy

| Гистологический тип<br>Histological type | Макс. диаметр, мкм<br>Max diameter, μm | Отношение меньшей оси эллипса к большей<br>Inverse aspect ratio of the ellipsis | Клеточная плотность, 1/мм$^2$<br>Cell density, 1/mm$^2$ | Клеточная плотность, 1/мкм$^3$<br>Cell density, 1/μm$^3$ |
|---|---|---|---|---|
| Нормальное белое вещество<br>Normal white matter | 4–5 [33] | - | 850.9 [32] | $0.025\times10^{-3}$ |
| Пилоцитарная астроцитома (степень I)<br>Pilocytic astrocytoma (Grade I) | - | - | 2689±745 [34] | $0.14\times10^{-3}$ |
| Диффузная астроцитома (степень II)<br>Diffuse astrocytoma (Grade II) | 8.93±1.26 [35] | 0.74±0.13 [36] | 2363±726 [37] | $0.12\times10^{-3}$ |
| Анапластическая астроцитома (степень III)<br>Anaplastic astrocytoma (Grade III) | 9.61±0.9 [27] | 0.65±0.15 [36] | 4864±1428 [37] | $0.34\times10^{-3}$ |
| Глиобластома (степень IV)<br>Glioblastoma (Grade IV) | 10.65±3.44 [35] | 0.627±0.5 [38] | 5540±2160 | $0.41\times10^{-3}$ |

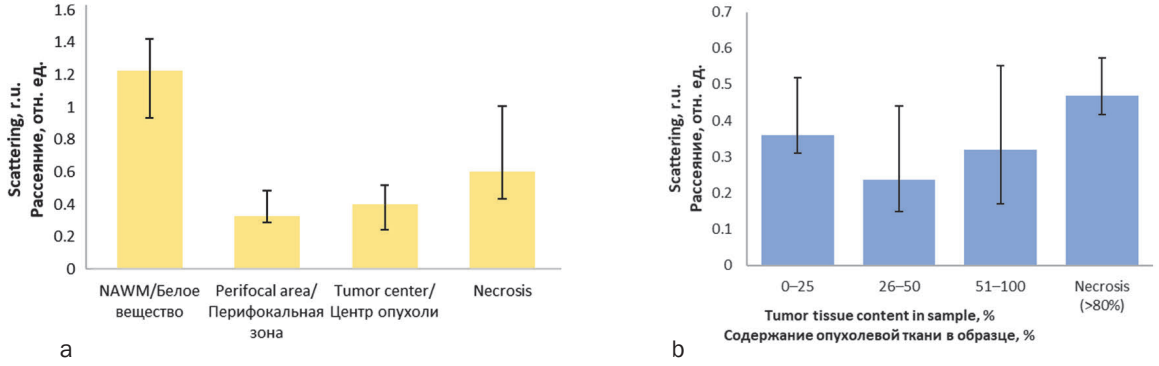


**Рис. 2.** Вариация индекса диффузного рассеяния в опухолевых тканях (представлен сигнал диффузного отражения на длине волны 632.8 нм), регистрируемая (a) интраоперационно *in vivo* и (b) на образцах из операционной *ex vivo*.
**Fig. 2.** Diffuse scattering index in tumor tissues (as scattering index at 632.8 nm) registered (a) intraoperatively *in vivo* and (b) in *ex vivo* samples.

***Comparison of results of mathematical modeling and spectroscopic measurements of gliomas***

Local changes in light-scattering properties and accumulation of tumor marker (5-ALA induced PpIX) in the patient's tissues during tumor removal were investigated. For this purpose, the data of spectroscopic study performed *in vivo* in different tumor sections were compared with the subsequent sampling of histological material from the same sections. As a result of the analysis of structural features of nervous tissues, and in particular healthy white matter of the brain and glial tumors of different degrees of malignancy, as well as physiological characteristics, a mathematical model of scattering signal formation in the tissues under study was created using Mie theory (Table 3). The optical parameters of the model composition media obtained as a result of modeling are shown in Table 4.

Comparison of the results of numerical modeling of laser radiation propagation in a complex medium that contains scatterers with parameters corresponding to the main structural elements of nervous tissues and hemoglobin as the main chromophore and the data of spectroscopic study carried out *in vivo* showed a good correspondence between the developed mathematical model and clinical data (Table 5).

As can be seen from the above results, both in numerical experiment and *in vivo* spectroscopic studies, differences in light-scattering properties were observed for the center and edge of tumor of different degrees of malignancy.

The light scattering of the central portion of benign neoplasms is less pronounced than that observed in glioblastoma. However, in both cases, this value is markedly lower than that exhibited by normal white matter. (Fig. 2). This can be explained by competing effects occurring at the tissue level during tumor development affecting the scattering signal. Gradual demyelination of nerve fibers, their displacement and destructurization, as well

**Таблица 3**
**Морфологические характеристики, послужившие входными данными для моделирования оптических свойств отдельных компонентов нервных тканей**

**Table 3**
**Morphological characteristics that served as input data for modeling the optical properties of individual components of neural tissues**

| Параметр Parameter | Центр Center | | | Край опухоли Tumor edge | | |
|---|---|---|---|---|---|---|
| | a, мкм a, μm | ρ, 1/мкм² ρ, 1/μm² | n | a, мкм a, μm | ρ, 1/мкм² ρ, 1/μm² | n |
| Норма Normal tissue | 4 / 0.5 / 0.8 (100%) | 0.0004 / 200 / 0.07 | 1.39 / 1.42 / 1.455 | - | | |
| Степень II–III Grade II–III | 9.5 / 0.3 / 0.8 (40%); 0.48 (60%*) | 0.0007 / 70 / 0.07 | 1.39 / 1.42 / 1.455 | 8.5 / 0.3 / 0.8 (50%); 0.48 (50%*) | 0.0005 / 70 / 0.07 | 1.39 / 1.42 /1.455 |
| Степень IV Grade IV | 10.65 / 0.25 / 0.8 (20%); 0.48 (80%*) | 0.0015 / 0-30 / 0.07 | 1.39 / 1.42 / 1.455 | 9.5 / 0.25 / 0.8 (40%); 0.48 (60%*) | 0.0007 / 30 / 0.07 | 1.39 / 1.42 /1.455 |

*$a$ – диаметр рассеивателя, $\rho$ – плотность ядер, $n$ – показатель преломления. Значения приведены для ядра / митохондрии / миелинизированных волокон.
*$a$ – diameter of scatterers, $\rho$ – nuclei density, $n$ – reflectance index. Values are provided for nucleus / mitochondria / myelinated fibers.

**Таблица 4**
**Оптические свойства нервных тканей с различной морфологией, полученные в результате математического моделирования с использованием многокомпонентной модели соответствующих тканей**
**Table 4**
**Optical properties of nervous tissues with different morphology obtained by mathematical modeling using a multi-component model of the corresponding tissues**

| Параметр Parameter | Длина волны, нм Wavelength, nm | Норма Normal tissue | Степень II–III Grade II–III | | Степень IV Grade IV | |
|---|---|---|---|---|---|---|
| | | | Центр опухоли Tumor center | Край опухоли Tumor edge | Центр опухоли Tumor center | Край опухоли Tumor edge |
| $\mu_s$, 1/см $\mu_s$, 1/cm | **632.8** | 113.7 | 49.7 | 54.2 | 112.6 | 50.9 |
| | **710** | 88.4 | 39.3 | 42.9 | 90 | 40.3 |
| $\mu_a$, 1/см $\mu_a$, 1/cm | **632.8** | 1.7 | 3 | 2.2 | 7.1 | 3.5 |
| | **710** | 0.76 | 2 | 1.5 | 2.5 | 1.2 |
| G | **632.8** | 0.85 | 0.89 | 0.86 | 0.9 | 0.89 |
| | **710** | 0.84 | 0.88 | 0.85 | 0.89 | 0.88 |

**Таблица 5**
**Сопоставление данных имитационного моделирования и результатов спектроскопии *in vivo***
**Table 5**
**Comparison of simulation results with *in vivo* spectroscopy**

| Диффузное отражение по отношению к нормальной ткани Diffuse reflectance compared to normal tissue | | Степень II–III Grade II–III | | Степень IV Grade IV | |
|---|---|---|---|---|---|
| | | Центр опухоли Tumor center | Край опухоли Tumor edge | Центр опухоли Tumor center | Край опухоли Tumor edge |
| Монте-Карло Monte Carlo | 632.8 нм 632.8 nm | 0.22±0.001 | 0.41±0.002 | 0.56±0.001 | 0.28±0.001 |
| *in vivo* | | 0.21±0.02 | 0.37±0.02 | 0.53±0.02 | 0.26±0.02 |

as a decrease in the number of mitochondria due to the transition of tumor cells from oxidative phosphorylation to glycolysis, lead to a decrease in the scattering signal, while an increase in the size and density of nuclei leads to its increase. For different parts of the tumor of one patient, this effect can be traced by comparing the central part of the tumor and its edge, where these changes are less pronounced than in the center. Here we see the opposite picture. The tumor edge of benign neoplasms exhibits higher scattering properties than the edge of glioblastoma, because in this region in the former case there is not yet significant destructurization of myelinated fibers and the decline of the scattering signal is due to the greatest extent to metabolic changes leading to the depletion of intracellular composition, while in the latter case all components leading to the decline of the scattering signal are already evident, but cellular density is not as pronounced as in the center of the tumor. Thus, we can rank the considered areas of pathologically altered tissues in the following order: normal white matter, edge of benign tumor, center of benign tumor, edge of malignant tumor, center of malignant tumor, which illustrates the competitive nature of parameters influencing the light scattering signal.

## Conclusion

The study of the scattering properties of glial tumors, both *in vivo* during neurosurgical operations and *ex vivo* during biobanking of the samples, showed that in the regions with low accumulation of tumor marker (5-ALA induced PpIX) and insignificant changes perceived visually, that the light scattering signal, registered at a small distance between the light source and the receiver and that mostly depends on the changes occurring at the subcellular level, has the highest contrast compared to the normal white matter of the brain. Thus, the diagnostic value of analyzing the light-scattering properties of neural tissues in the perifocal zone of glial tumors has been demonstrated.

*This work was financially supported by the Ministry of Science and Higher Education of the Russian Federation (Agreement No. 075-15-2021-1343 dated October 4, 2021).*

## REFERENCES


1. Vasefi F., MacKinnon N., Farkas D. L. et al. Review of the potential of optical technologies for cancer diagnosis in neurosurgery: a step toward intraoperative neurophotonics, *Neurophotonics*, 2016, vol. 4(1), pp. 011010. doi: 10.1117/1.NPh.4.1.011010.
2. Goryaynov S. A., Okhlopkov V. A., Golbin D. A. et al. Fluorescence Diagnosis in Neurooncology: Retrospective Analysis of 653 Cases, *Frontiers in Oncology*, 2019, vol. 9, pp. 830. doi: 10.3389/fonc.2019.00830.
3. Goryaynov S. A., Buklina S. B., Khapov I. V. et al. 5-ALA-guided tumor resection during awake speech mapping in gliomas located in eloquent speech areas: Single-center experience, *Frontiers in Oncology*, 2022, vol. 12, pp. 940951. doi: 10.3389/fonc.2022.940951.
4. Rynda A. Yu., Olyushin V. E., Rostovtsev D. M. et al. Fluorescent diagnostics with chlorin e6 in surgery of low-grade glioma, *Biomedical Photonics*, 2021, vol. 10(4), pp. 35–43. doi: 10.24931/2413-9432-2021-10-4-35-43.
5. Rynda A. Yu., Olyushin V. E., Rostovtsev D. M. et al. Results of microsurgical resection of glioblastomas under endoscopic and fluorescent control, *Biomedical Photonics*, 2024, vol. 13(3), pp. 20–30. doi: 10.24931/2413-9432-2024-13-3-20-30.
6. Udeneev A. M., Kalyagina N. A., Reps V. F. et al. Photo and spectral fluorescence analysis of the spinal cord injury area in animal models, *Biomedical Photonics*, 2023, vol. 12(3), pp. 15–20. doi: 10.24931/2413-9432-2023-12-3-16-20.
7. Liu Y.-X., Yang Y.-S. Using Diffuse Reflectance Spectroscopy to Classify Tumor Tissue in Upper Gastrointestinal Cancers, *JAMA Surgery*, 2023, vol. 158(7), pp. 772. doi: 10.1001/jamasurg.2022.8430.
8. Baltussen E. J. M., Brouwer De Koning S. G., Sanders J. et al. Using Diffuse Reflectance Spectroscopy to Distinguish Tumor Tissue From Fibrosis in Rectal Cancer Patients as a Guide to Surgery, *Lasers in Surgery and Medicine*, 2020, vol. 52(7), pp. 604–611. doi: 10.1002/lsm.23196.
9. Grosenick D., Wabnitz H., Macdonald R. Diffuse near-infrared imaging of tissue with picosecond time resolution, *Biomedical Engineering / Biomedizinische Technik*, 2018, vol. 63(5), pp. 511–518. doi: 10.1515/bmt-2017-0067.
10. Rejmstad P., Johansson J. D., Haj-Hosseini N. et al. A method for monitoring of oxygen saturation changes in brain tissue using diffuse reflectance spectroscopy, *Journal of Biophotonics*, 2017, vol. 10(3), pp. 446–455. doi: 10.1002/jbio.201500334.
11. Skyrman S., Burström G., Lai M. et al. Diffuse reflectance spectroscopy sensor to differentiate between glial tumor and healthy brain tissue: a proof-of-concept study, *Biomedical Optics Express*, 2022, vol. 13(12), pp. 6470. doi: 10.1364/BOE.474344.
12. Li K., Wu Q., Feng S. et al. In situ detection of human glioma based on tissue optical properties using diffuse reflectance spectroscopy, *Journal of Biophotonics*, 2023, vol. 16(11), pp. e202300195. doi: 10.1002/jbio.202300195.
13. Potapov A. A., Goriaĭnov S. A., Loshchenov V. B. et al. Intraoperative combined spectroscopy (optical biopsy) of cerebral gliomas, *Zhurnal Voprosy Neirokhirurgii Imeni N.N. Burdenko*, 2013, vol. 77(2), pp. 3–10.
14. Romanishkin I., Savelieva T., Kosyrkova A. et al. Differentiation of glioblastoma tissues using spontaneous Raman scattering with dimensionality reduction and data classification, *Frontiers in Oncology*, 2022, vol. 12, pp. 944210. doi: 10.3389/fonc.2022.944210.
15. Ospanov A., Romanishkin I., Savelieva T. et al. Optical Differentiation of Brain Tumors Based on Raman Spectroscopy and Cluster Analysis Methods, *International Journal of Molecular Sciences*, 2023, vol. 24(19), pp. 14432. doi: 10.3390/ijms241914432.
16. Romanishkin I. D., Savelieva T. A., Ospanov A. et al. Classification of intracranial tumors based on optical-spectral analysis, *Biomedical Photonics*, 2023, vol. 12(3), pp. 4–10. doi: 10.24931/2413-9432-2023-12-3-4-10.
17. Stratonnikov A. A., Meerovich G. A., Ryabova A. V. et al. Application of backward diffuse reflection spectroscopy for monitoring the state of tissues in photodynamic therapy, *Quantum Electronics*, 2006, vol. 36(12), pp. 1103–1110. doi: 10.1070/QE2006v036n12ABEH013331.
18. Pominova D. V., Ryabova A. V., Skobeltsin A. S. et al. Spectroscopic study of methylene blue *in vivo*: effects on tissue oxygenation and tumor metabolism, *Biomedical Photonics*, 2023, vol. 12(1), pp. 4–13. doi: 10.24931/2413-9432-2023-12-1-4-13.
19. Jacques S. L., Pogue B. W. Tutorial on diffuse light transport, *Journal of Biomedical Optics*, 2008, vol. 13(4), pp. 041302. doi: 10.1117/1.2967535.
20. Bohren C. F., Huffman D. R. Absorption and Scattering of Light by Small Particles / C. F. Bohren, D. R. Huffman, 1 ed., Wiley, 1998. doi: 10.1002/9783527618156.
21. Wang L., Jacques S. L., Zheng L. MCML—Monte Carlo modeling of light transport in multi-layered tissues, *Computer Methods and Programs in Biomedicine*, 1995, vol. 47(2), pp. 131–146. doi: 10.1016/0169-2607(95)01640-F.


## ЛИТЕРАТУРА


1. Vasefi F., MacKinnon N., Farkas D. L. et al. Review of the potential of optical technologies for cancer diagnosis in neurosurgery: a step toward intraoperative neurophotonics // Neurophotonics. – 2016. – Vol. 4. – № 1. – P. 011010.doi: 10.1117/1.NPh.4.1.011010.
2. Goryaynov S. A., Okhlopkov V. A., Golbin D. A. et al. Fluorescence Diagnosis in Neurooncology: Retrospective Analysis of 653 Cases // Frontiers in Oncology. – 2019. – Vol. 9. – P. 830.doi: 10.3389/fonc.2019.00830.
3. Goryaynov S. A., Buklina S. B., Khapov I. V. et al. 5-ALA-guided tumor resection during awake speech mapping in gliomas located in eloquent speech areas: Single-center experience // Frontiers in Oncology. – 2022. – Vol. 12. – P. 940951.doi: 10.3389/fonc.2022.940951.
4. Rynda A. Yu., Olyushin V. E., Rostovtsev D. M. et al. Fluorescent diagnostics with chlorin e6 in surgery of low-grade glioma // Biomedical Photonics. – 2021. – Vol. 10. – № 4. – P. 35–43.doi: 10.24931/2413-9432-2021-10-4-35-43.
5. Rynda A. Yu., Olyushin V. E., Rostovtsev D. M. et al. Results of microsurgical resection of glioblastomas under endoscopic and fluorescent control // Biomedical Photonics. – 2024. – Vol. 13. – № 3. – P. 20–30.doi: 10.24931/2413-9432-2024-13-3-20-30.
6. Udeneev A. M., Kalyagina N. A., Reps V. F. et al. Photo and spectral fluorescence analysis of the spinal cord injury area in animal models // Biomedical Photonics. – 2023. – Vol. 12. – № 3. – P. 15–20.doi: 10.24931/2413-9432-2023-12-3-16-20.
7. Liu Y.-X., Yang Y.-S. Using Diffuse Reflectance Spectroscopy to Classify Tumor Tissue in Upper Gastrointestinal Cancers // JAMA Surgery. – 2023. – Vol. 158. – № 7. – P. 772.doi: 10.1001/jamasurg.2022.8430.
8. Baltussen E. J. M., Brouwer De Koning S. G., Sanders J. et al. Using Diffuse Reflectance Spectroscopy to Distinguish Tumor Tissue From Fibrosis in Rectal Cancer Patients as a Guide to Surgery // Lasers in Surgery and Medicine. – 2020. – Vol. 52. – № 7. – P. 604–611.doi: 10.1002/lsm.23196.
9. Grosenick D., Wabnitz H., Macdonald R. Diffuse near-infrared imaging of tissue with picosecond time resolution // Biomedical Engineering / Biomedizinische Technik. – 2018. – Vol. 63. – № 5. – P. 511–518.doi: 10.1515/bmt-2017-0067.
10. Rejmstad P., Johansson J. D., Haj-Hosseini N. et al. A method for monitoring of oxygen saturation changes in brain tissue using diffuse reflectance spectroscopy // Journal of Biophotonics. – 2017. – Vol. 10. – № 3. – P. 446–455.doi: 10.1002/jbio.201500334.
11. Skyrman S., Burström G., Lai M. et al. Diffuse reflectance spectroscopy sensor to differentiate between glial tumor and healthy brain tissue: a proof-of-concept study // Biomedical Optics Express. – 2022. – Vol. 13. – № 12. – P. 6470.doi: 10.1364/BOE.474344.
12. Li K., Wu Q., Feng S. et al. In situ detection of human glioma based on tissue optical properties using diffuse reflectance spectroscopy // Journal of Biophotonics. – 2023. – Vol. 16. – № 11. – P. e202300195.doi: 10.1002/jbio.202300195.
13. Potapov A. A., Goriaĭnov S. A., Loshchenov V. B. et al. Intraoperative combined spectroscopy (optical biopsy) of cerebral gliomas // Zhurnal Voprosy Neirokhirurgii Imeni N.N. Burdenko. – 2013. – Vol. 77. – № 2. – P. 3–10.
14. Romanishkin I., Savelieva T., Kosyrkova A. et al. Differentiation of glioblastoma tissues using spontaneous Raman scattering with dimensionality reduction and data classification // Frontiers in Oncology. – 2022. – Vol. 12. – P. 944210.doi: 10.3389/fonc.2022.944210.
15. Ospanov A., Romanishkin I., Savelieva T. et al. Optical Differentiation of Brain Tumors Based on Raman Spectroscopy and Cluster Analysis Methods // International Journal of Molecular Sciences. – 2023. – Vol. 24. – № 19. – P. 14432.doi: 10.3390/ijms241914432.
16. Romanishkin I. D., Savelieva T. A., Ospanov A. et al. Classification of intracranial tumors based on optical-spectral analysis // Biomedical Photonics. – 2023. – Vol. 12. – № 3. – P. 4–10.doi: 10.24931/2413-9432-2023-12-3-4-10.
17. Stratonnikov A. A., Meerovich G. A., Ryabova A. V. et al. Application of backward diffuse reflection spectroscopy for monitoring the state of tissues in photodynamic therapy // Quantum Electronics. – 2006. – Vol. 36. – № 12. – P. 1103–1110.doi: 10.1070/QE2006v036n12ABEH013331.
18. Pominova D. V., Ryabova A. V., Skobeltsin A. S. et al. Spectroscopic study of methylene blue *in vivo*: effects on tissue oxygenation and tumor metabolism // Biomedical Photonics. – 2023. – Vol. 12. – № 1. – P. 4–13. doi: 10.24931/2413-9432-2023-12-1-4-13.
19. Jacques S. L., Pogue B. W. Tutorial on diffuse light transport // Journal of Biomedical Optics. – 2008. – Vol. 13. – № 4. – P. 041302.doi: 10.1117/1.2967535.
20. Bohren C. F., Huffman D. R. Absorption and Scattering of Light by Small Particles / C. F. Bohren, D. R. Huffman, 1., Wiley, 1998.doi: 10.1002/9783527618156.
21. Wang L., Jacques S. L., Zheng L. MCML—Monte Carlo modeling of light transport in multi-layered tissues // Computer Methods and Programs in Biomedicine. – 1995. – Vol. 47. – № 2. – P. 131–146.doi: 10.1016/0169-2607(95)01640-F.

22. Evolution of the Molecular Biology of Brain Tumors and the Therapeutic Implications ed. T. Lichtor, InTech, 2013. doi: 10.5772/50198.
23. Giese A., Bjerkvig R., Berens M. E. et al. Cost of Migration: Invasion of Malignant Gliomas and Implications for Treatment, *Journal of Clinical Oncology*, 2003, vol. 21(8), pp. 1624–1636. doi: 10.1200/JCO.2003.05.063.
24. Wang S., Meng M., Zhang X. et al. Texture analysis of diffusion weighted imaging for the evaluation of glioma heterogeneity based on different regions of interest, *Oncology Letters*, 2018 doi: 10.3892/ol.2018.8232.
25. Brunberg J. A., Chenevert T. L., McKeever P. E. et al. *In vivo* MR determination of water diffusion coefficients and diffusion anisotropy: correlation with structural alteration in gliomas of the cerebral hemispheres, *AJNR. American journal of neuroradiology*, 1995, vol. 16(2), pp. 361–371.
26. Sinha S., Bastin M. E., Whittle I. R. et al. Diffusion tensor MR imaging of high-grade cerebral gliomas, *AJNR. American journal of neuroradiology*, 2002, vol. 23(4), pp. 520–527.
27. Johansen-Berg H., Behrens T. E. J. Diffusion MRI: from quantitative measurement to in-vivo neuroanatomy / H. Johansen-Berg, T. E. J. Behrens, 1st ed ed., Amsterdam Boston: Elsevier/Academic Press, 2009.
28. Basic neurochemistry: principles of molecular, cellular, and medical neurobiology ed. S. T. Brady, G. J. Siegel, R. W. Albers et al., 8th ed ed., Amsterdam: Academic Press, 2012. 1 c.
29. Le Bihan D., Mangin J., Poupon C. et al. Diffusion tensor imaging: Concepts and applications, *Journal of Magnetic Resonance Imaging*, 2001, vol. 13(4), pp. 534–546. doi: 10.1002/jmri.1076.
30. Lu S., Ahn D., Johnson G. et al. Peritumoral diffusion tensor imaging of high-grade gliomas and metastatic brain tumors, *AJNR. American journal of neuroradiology*, 2003, vol. 24(5), pp. 937–941.
31. Goebell E., Paustenbach S., Vaeterlein O. et al. Low-Grade and Anaplastic Gliomas: Differences in Architecture Evaluated with Diffusion-Tensor MR Imaging, *Radiology*, 2006, vol. 239(1), pp. 217–222. doi: 10.1148/radiol.2383050059.
32. Cotter D., Mackay D., Landau S. et al. Reduced Glial Cell Density and Neuronal Size in the Anterior Cingulate Cortex in Major Depressive Disorder, *Archives of General Psychiatry*, 2001, vol. 58(6), pp. 545. doi: 10.1001/archpsyc.58.6.545.
33. Spacek J. Atlas of Ultrastructural Neurocytology at SynapseWeb [Website]. URL: https://synapseweb.clm.utexas.edu/atlas (accessed: 18.11.2024).
34. Cruz-Sánchez F. F., Ferreres J. C., Figols J. et al. Prognostic analysis of astrocytic gliomas correlating histological parameters with the proliferating cell nuclear antigen labelling index (PCNA-LI), *Histology and Histopathology*, 1997, vol. 12(1), pp. 43–49.
35. Nafe R., Schlote W. Densitometric Analysis of Tumor Cell Nuclei in lowgrade and high-grade Astrocytomas, *Electronic Journal of Pathology and Histology*, 2002, vol. 8(3).
36. Candolfi M., Curtin J. F., Nichols W. S. et al. Intracranial glioblastoma models in preclinical neuro-oncology: neuropathological characterization and tumor progression, *Journal of Neuro-Oncology*, 2007, vol. 85(2), pp. 133–148. doi: 10.1007/s11060-007-9400-9.
37. Nafe R., Herminghaus S., Pilatus U. et al. Morphology of proliferating and non-proliferating tumor cell nuclei in glioblastomas correlates with preoperative data from proton-MR-spectroscopy, *Neuropathology*, 2004, vol. 24(3), pp. 172–182. doi: 10.1111/j.1440-1789.2004.00547.x.
38. Schiffer Astrocytic Tumors I Berlin/Heidelberg: Springer-Verlag, 2006.p. 27–58. doi: 10.1007/1-4020-3998-0_5.
39. Sarkar C., Jain A., Suri V. Current concepts in the pathology and genetics of gliomas, *Indian Journal of Cancer*, 2009, vol. 46(2), pp. 108. doi: 10.4103/0019-509X.49148.
40. Pysh J. J., Khan T. Variations in mitochondrial structure and content of neurons and neuroglia in rat brain: An electron microscopic study, *Brain Research*, 1972, vol. 36(1), pp. 1–18. doi: 10.1016/0006-8993(72)90762-7.
41. Beauvoit B., Evans S. M., Jenkins T. W. et al. Correlation Between the Light Scattering and the Mitochondrial Content of Normal Tissues and Transplantable Rodent Tumors, *Analytical Biochemistry*, 1995, vol. 226(1), pp. 167–174. doi: 10.1006/abio.1995.1205.
42. Beauvoit B., Kitai T., Chance B. Contribution of the mitochondrial compartment to the optical properties of the rat liver: a theoretical and practical approach, *Biophysical Journal*, 1994, vol. 67(6), pp. 2501–2510. doi: 10.1016/S0006-3495(94)80740-4.
43. Beauvoit B., Chance B. Time-Resolved Spectroscopy of mitochondria, cells and tissues under normal and pathological conditions, *Molecular and Cellular Biochemistry*, 1998, vol. 184(1/2), pp. 445–455. doi: 10.1023/A:1006855716742.
44. Schmitt J. M., Kumar G. Turbulent nature of refractive-index variations in biological tissue, *Optics Letters*, 1996, vol. 21(16), pp. 1310. doi: 10.1364/OL.21.001310.

22. Evolution of the Molecular Biology of Brain Tumors and the Therapeutic Implications ed. T. Lichtor, InTech, 2013.doi: 10.5772/50198.
23. Giese A., Bjerkvig R., Berens M. E. et al. Cost of Migration: Invasion of Malignant Gliomas and Implications for Treatment // Journal of Clinical Oncology. – 2003. – Vol. 21. – № 8. – P. 1624–1636.doi: 10.1200/JCO.2003.05.063.
24. Wang S., Meng M., Zhang X. et al. Texture analysis of diffusion weighted imaging for the evaluation of glioma heterogeneity based on different regions of interest // Oncology Letters. – 2018.doi: 10.3892/ol.2018.8232.
25. Brunberg J. A., Chenevert T. L., McKeever P. E. et al. *In vivo* MR determination of water diffusion coefficients and diffusion anisotropy: correlation with structural alteration in gliomas of the cerebral hemispheres // AJNR. American journal of neuroradiology. – 1995. – Vol. 16. – № 2. – P. 361–371.
26. Sinha S., Bastin M. E., Whittle I. R. et al. Diffusion tensor MR imaging of high-grade cerebral gliomas // AJNR. American journal of neuroradiology. – 2002. – Vol. 23. – № 4. – P. 520–527.
27. Johansen-Berg H., Behrens T. E. J. Diffusion MRI: from quantitative measurement to in-vivo neuroanatomy / H. Johansen-Berg, T. E. J. Behrens, 1st ed., Amsterdam Boston: Elsevier/Academic Press, 2009.
28. Basic neurochemistry: principles of molecular, cellular, and medical neurobiology ed. S. T. Brady, G. J. Siegel, R. W. Albers et al., 8th ed., Amsterdam: Academic Press, 2012. 1 c.
29. Le Bihan D., Mangin J., Poupon C. et al. Diffusion tensor imaging: Concepts and applications // Journal of Magnetic Resonance Imaging. – 2001. – Vol. 13. – № 4. – P. 534–546.doi: 10.1002/jmri.1076.
30. Lu S., Ahn D., Johnson G. et al. Peritumoral diffusion tensor imaging of high-grade gliomas and metastatic brain tumors // AJNR. American journal of neuroradiology. – 2003. – Vol. 24. – № 5. – P. 937–941.
31. Goebell E., Paustenbach S., Vaeterlein O. et al. Low-Grade and Anaplastic Gliomas: Differences in Architecture Evaluated with Diffusion-Tensor MR Imaging // Radiology. – 2006. – Vol. 239. – № 1. – P. 217–222.doi: 10.1148/radiol.2383050059.
32. Cotter D., Mackay D., Landau S. et al. Reduced Glial Cell Density and Neuronal Size in the Anterior Cingulate Cortex in Major Depressive Disorder // Archives of General Psychiatry. – 2001. – Vol. 58. – № 6. – P. 545.doi: 10.1001/archpsyc.58.6.545.
33. Spacek J. Atlas of Ultrastructural Neurocytology at SynapseWeb [Электронный ресурс]. URL: https://synapseweb.clm.utexas.edu/atlas (accessed: 18.11.2024).
34. Cruz-Sánchez F. F., Ferreres J. C., Figols J. et al. Prognostic analysis of astrocytic gliomas correlating histological parameters with the proliferating cell nuclear antigen labelling index (PCNA-LI) // Histology and Histopathology. – 1997. – Vol. 12. – № 1. – P. 43–49.
35. Nafe R., Schlote W. Densitometric Analysis of Tumor Cell Nuclei in lowgrade and high-grade Astrocytomas // Electronic Journal of Pathology and Histology. – 2002. – Vol. 8. – № 3.
36. Candolfi M., Curtin J. F., Nichols W. S. et al. Intracranial glioblastoma models in preclinical neuro-oncology: neuropathological characterization and tumor progression // Journal of Neuro-Oncology. – 2007. – Vol. 85. – № 2. – P. 133–148.doi: 10.1007/s11060-007-9400-9.
37. Nafe R., Herminghaus S., Pilatus U. et al. Morphology of proliferating and non-proliferating tumor cell nuclei in glioblastomas correlates with preoperative data from proton-MR-spectroscopy // Neuropathology. – 2004. – Vol. 24. – № 3. – P. 172–182.doi: 10.1111/j.1440-1789.2004.00547.x.
38. Schiffer Astrocytic Tumors I Berlin/Heidelberg: Springer-Verlag, 2006. C. 27–58.doi: 10.1007/1-4020-3998-0_5.
39. Sarkar C., Jain A., Suri V. Current concepts in the pathology and genetics of gliomas // Indian Journal of Cancer. – 2009. – Vol. 46. – № 2. – P. 108. doi: 10.4103/0019-509X.49148.
40. Pysh J. J., Khan T. Variations in mitochondrial structure and content of neurons and neuroglia in rat brain: An electron microscopic study // Brain Research. – 1972. – Vol. 36. – № 1. – P. 1–18. doi: 10.1016/0006-8993(72)90762-7.
41. Beauvoit B., Evans S. M., Jenkins T. W. et al. Correlation Between the Light Scattering and the Mitochondrial Content of Normal Tissues and Transplantable Rodent Tumors // Analytical Biochemistry. – 1995. – Vol. 226. – № 1. – P. 167–174.doi: 10.1006/abio.1995.1205.
42. Beauvoit B., Kitai T., Chance B. Contribution of the mitochondrial compartment to the optical properties of the rat liver: a theoretical and practical approach // Biophysical Journal. – 1994. – Vol. 67. – № 6. – P. 2501–2510.doi: 10.1016/S0006-3495(94)80740-4.
43. Beauvoit B., Chance B. Time-Resolved Spectroscopy of mitochondria, cells and tissues under normal and pathological conditions // Molecular and Cellular Biochemistry. – 1998. – Vol. 184. – № 1/2. – P. 445–455.doi: 10.1023/A:1006855716742.
44. Schmitt J. M., Kumar G. Turbulent nature of refractive-index variations in biological tissue // Optics Letters. – 1996. – Vol. 21. – № 16. – P. 1310. doi: 10.1364/OL.21.001310.